Journal of Physiology (1989), **419**, *pp.* 627–650
With 12 text-figures
Printed in Great Britain

KINETIC PROPERTIES OF THE CARDIAC T-TYPE CALCIUM CHANNEL IN THE GUINEA-PIG

BY G. DROOGMANS AND B. NILIUS

From the Laboratorium voor Fysiologie, Campus Gasthuisberg Katholieke Universiteit Leuven, B-3000 Leuven, Belgium and the Julius Bernstein Institut für Physiologie, Martin Luther Universität Halle Wittenberg, DDR-4010 Halle (Saale), GDR

(*Received 13 February 1989*)

SUMMARY

1. The kinetic properties of T-type Ca^{2+} channels were examined in single ventricular cells from guinea-pig hearts using the cell-attached configuration of the patch-clamp technique.

2. T-type Ca^{2+} channel activity has been observed in 44 out of 139 patches. The density of these channels was estimated at 0·1–0·3 μm^{-2}. The T-type Ca^{2+} channel responds to a depolarizing voltage step either with a burst of openings which appears with a distinct delay or with no openings at all. The mean number of bursts per record for the records showing channel activity is 1·1. The probability of observing a blank sweep is high and amounts to $0{\cdot}65 \pm 0{\cdot}02$ ($n = 26$).

3. With 110 mM-Ca^{2+} in the pipette solution, the slope conductance calculated from the current–voltage relationship of the single-channel current in the range between -50 and $+10$ mV is 6·8 pS.

4. Openings to a subconductance level of about 50% of the main level could be resolved. All possible transitions between the subconductance and the main level were observed, indicating that the cardiac T-type Ca^{2+} channel possesses a substate.

5. The macroscopic steady-state activation and inactivation, as determined from ensemble-averaged currents, could be described by Boltzmann functions. Half-maximal activation and inactivation occur at -14 and $-60{\cdot}7$ mV, the slope parameters of these curves are 10·8 and 5·6 mV respectively. The maximum (peak) open probability is 0·15.

6. The ensemble-averaged current decays monoexponentially. The time constant is strongly voltage dependent and decreases at less negative potentials.

7. The open times are monoexponentially distributed. The mean open time of the channel does not depend on either the holding or the test potential, and has a mean value of 1·4 ms. The distribution of the closed times is biexponential. The fast mean closed time is also voltage independent with a mean value of 0·48 ms. The slow mean closed time increases with voltage from 1·9 ms at -40 mV to 8·8 ms at 0 mV. The mean burst duration also increases with voltage from a value of 4·9 ms at -40 mV to 13·9 ms at -10 mV.

8. The convolution of the first-latency distribution with that of the burst duration

closely fits the open probability calculated from the ensemble-averaged current. The mean first latency is also closely correlated with the macroscopic time constant of inactivation. It was strongly voltage dependent, and decreased from a value 41 ms at −50 mV to 9·1 ms at 0 mV.

9. The microscopic kinetics of the T-type Ca^{2+} channel is characterized by a high and voltage-independent probability of reopening $p = 0{\cdot}8 \pm 0{\cdot}01$ ($n = 26$). The probability f that the channel bypasses the open state is 0·84 at −40 mV, reaches a minimum value of 0·52 at −30 mV and increases again at more positive values (0·74 at 0 mV). The number of openings per non-empty sweep is only weakly voltage dependent with a mean value of $4{\cdot}7 \pm 0{\cdot}3$ openings per sweep.

10. The high probabilities with which the channel reopens and bypasses the open state can be described by a model in which inactivation occurs from a closed state. The strong correlation between first latency and time constant of macroscopic inactivation on the other hand indicate that inactivation might occur from the open state. Our analysis does not, however, discriminate between kinetic schemes with inactivation coupled to or independent of activation.

INTRODUCTION

The existence of multiple types of Ca^{2+} channels in heart muscle is widely accepted (Bean, 1985; Nilius, Hess, Lansman & Tsien, 1985, 1986; Bonvallet, 1987; Hagiwara, Irisawa & Kameyama, 1988) and fits with the increasing amount of evidence that several types of Ca^{2+} channels co-exist in various excitable cells (see McCleskey, Fox, Feldman & Tsien, 1986 for a review). In contrast with the L-type or 'high threshold' Ca^{2+} channel, the T-type (Nilius *et al.* 1985) or 'low threshold' (Carbone & Lux, 1984) Ca^{2+} channel has a smaller conductance, it activates at potentials ranging from −50 to −30 mV, shows a fast inactivation, and is insensitive to 1,4-dihydropyridines. It further shows a high affinity block by nickel ions and it is not dependent on a cyclic AMP-mediated phosphorylation (Nilius *et al.* 1985; Fox, Nowycky & Tsien, 1987*a*, *b*; Hagiwara *et al.* 1988; Tytgat, Nilius, Vereecke & Carmeliet, 1988). These properties seem to be common to T-type Ca^{2+} channels observed in a large variety of excitable tissues.

Although the T-type Ca^{2+} channel can be clearly distinguished from other ionic channels in heart, its functional importance remains unclear. Up to now there is only rather weak evidence that this channel might be involved in the regulation of rhythmic activity in heart and neuronal cells (Llinás & Yarom, 1981; Nilius, 1986; Hagiwara *et al.* 1988), in the regulation of hormone secretion (Cota, 1986; De Riemer & Sakmann, 1986; Hiriart & Matteson, 1988; Satin & Cook, 1988), and in the control of muscle activity or subcellular events (Deitmer, 1984; Mackie & Meech, 1985; Mitra & Morad, 1986).

In the present paper we have investigated the kinetic properties of the T-type Ca^{2+} channel at the single-channel level to evaluate the voltage dependence of the single-channel characteristics and to elucidate the mechanism of the voltage-dependent inactivation. The kinetics of the channel are described in terms of state models. Most

of the alternative models could be excluded by considering the reopening properties of the channel.

METHODS

The experiments were performed on single ventricular cells enzymatically isolated from guinea-pig hearts. Guinea-pigs were killed by a blow on the head, and single ventricular myocytes were dissociated by an enzymic dispersion similar to the one described in more detail by Mitra & Morad (1985). In three experiments we have used isolated atrial cells. T-channel activity in these cells was not different from that observed in ventricular cells, except that channel activity after seal formation was observed more frequently in the atrial cells.

All experiments were performed at 22 ± 1 °C.

Solutions

After isolation, the cells were stored in a HEPES-buffered solution that contained (mM): 140 NaCl, 1·8 $CaCl_2$, 5·4 KCl, 2 $MgCl_2$, 10 HEPES titrated with NaOH to pH 7. During the experiments the cells were depolarized to ≈ 0 mV by bathing them in an extracellular solution that contained (in mM): 140 potassium aspartate, 2 $MgCl_2$, 10 EGTA, 2 ATP, 10 HEPES titrated with KOH to pH 7·2. The pipette solution contained (mM): 110 $CaCl_2$, 10 HEPES titrated with $Ca(OH)_2$ to a pH of 7. In a few experiments a similar solution with 110 mM-$BaCl_2$ was used.

Current measurements

Single-channel currents were measured exclusively in the cell-attached mode of the patch-clamp technique (Hamill, Marty, Neher, Sakmann & Sigworth, 1981). Gigaseals were obtained using borosilicate micropipettes coated with Sylgard in order to reduce the capacitive transients. Because of the low density of T-type Ca^{2+} channels we have used pipettes with a resistance of about 1 MΩ, corresponding to an open tip area of about 3 μm^2 (Sakmann & Neher, 1983).

Voltage steps lasting 150 ms were delivered through a pulse generator at a frequency of 1 s^{-1}. The currents were filtered at 2 kHz with an 8-pole Bessel filter, and digitized at intervals of 150 μs using a 12-bit analog-to-digital converter. Each trace contained 1024 samples and usually 194 records were sampled at each test potential. Capacitive and leakage currents were largely eliminated by averaging records free of channel openings and subtracting this average from all the records. The seals in 110 mM-Ca^{2+} were very stable and baseline correction was not necessary.

Amplitude histograms were obtained from the digitized current records without fitting a mean amplitude to the individual channel openings. The counts in each bin were divided by the total number of points and by the bin width. The resulting values are probability densities, and were plotted *versus* the current amplitude. Amplitudes of single-channel currents were obtained by fitting the amplitude histograms to sums of Gaussian functions.

Idealized records were obtained from the digitized records by setting a transition threshold at half the amplitude of the unitary current. Open- and closed-time histograms and first-latency histograms (waiting time to the first opening per sweep) were calculated from the idealized records and fitted to sums of exponentials. The Simplex method was used to minimize the weighted sum of squares of the deviations between observed and expected bin frequencies. Each bin was weighted with the inverse of the theoretical value.

A histogram of the burst durations was calculated by defining a minimum interburst interval of three times the fast time constant of the closed-time histogram. We have not tried to calculate an optimal value for this parameter from the distributions of fast and slow closed times, because of the large variability in the estimated values of the slow time constant (mainly due to the limited number of observed closings in this time range). This somewhat arbitrary definition of the minimum interburst interval guarantees that less than 5% of the fast closings will be misinterpreted as interburst gaps. It will be shown below that the burst duration determined from the histogram is in good agreement with the predicted value calculated from the distributions of open and fast closings.

It was not possible to analyse the histograms for the burst duration and first latency at each test potential. We have therefore calculated the mean values of these parameters from the idealized records. All kinetic data were obtained from the twenty-nine patches that showed single-channel activity, so that no correction for the number of channels in a patch was required.

Evaluation of the number of openings per record

Kunze, Lacerda, Wilson & Brown (1985) have proposed a method to discriminate between different kinetic schemes based on the probability of finding zero openings and on the probability of reopening of the channel. From the records without openings and from the total number of openings the 'apparent' probability $P_A(0)$ of finding zero openings in a record and the mean number of 'apparent' openings per record j were calculated from

$$P_A(0) = \text{number of nulls/number of sweeps},$$
$$j = \text{number of openings/number of sweeps}.$$

The probability p that the channel reopens as well as the probability $P(0)$ of finding a 'null' can be obtained from these apparent values after correction for missed fast openings by taking into account the measured dead time $t_D = 170\ \mu s$ of our recording system, using the equations (Kunze *et al.* (1985)

$$p = (j-1+P_A(0))/(j+(P_A(0)-1)(1-P_D)),$$

and

$$P(0) = (P_A(0)-G)/(1-G),$$

$$G = (1-p)(1-P_D)/(1-p-pP_D),$$

where $P_D = \exp(-t_D/\tau_0)$ represents the probability of detecting a channel opening.

The predicted distribution of the number of openings per record based on these parameters will be compared to the experimental data.

Model approximation

We have tried to describe the microscopic kinetics of the cardiac T-type Ca^{2+} channel using different state models. Rate constants and transition probabilities for the various models were obtained from the open probabilities $P(t)$, i.e. the ensemble-averaged current normalized by the amplitude of the single-channel current. The numerical solution of the differential equations, which describe a particular model, were fitted to a smoothed form of $P(t)$. A Runge–Kutta method for the solution of a system of differential equations was combined with a Levenberg–Marquardt least-squares fitting routine.

Statistics

Pooled data are always given as means ± S.E.M.

RESULTS

Single-channel measurements of cardiac T-type Ca^{2+} channel

Single-channel activity of T-type Ca^{2+} channels in heart muscle was recorded under the following experimental conditions: (i) 110 mM-$CaCl_2$ in the patch pipette to discriminate between L- and T-channel activity; (ii) the use of pipettes with a wide tip diameter (resistance $\approx$ 1 MΩ).

Figure 1 shows some representative records of T- and L-channel currents. Panel *A* depicts channel openings under the conditions used in this study with 110 mM-$CaCl_2$ in the pipette. Short bursts of openings cluster at the beginning of the depolarizing voltage step, but sometimes also occur with a substantial delay from the beginning of the pulse (long first latency or waiting time for the first opening). The amplitude of the current is about 0·5 pA at −20 mV. The ensemble-averaged current, shown at the bottom of the panel, is transient. In contrast, L-type Ca^{2+} channels recorded

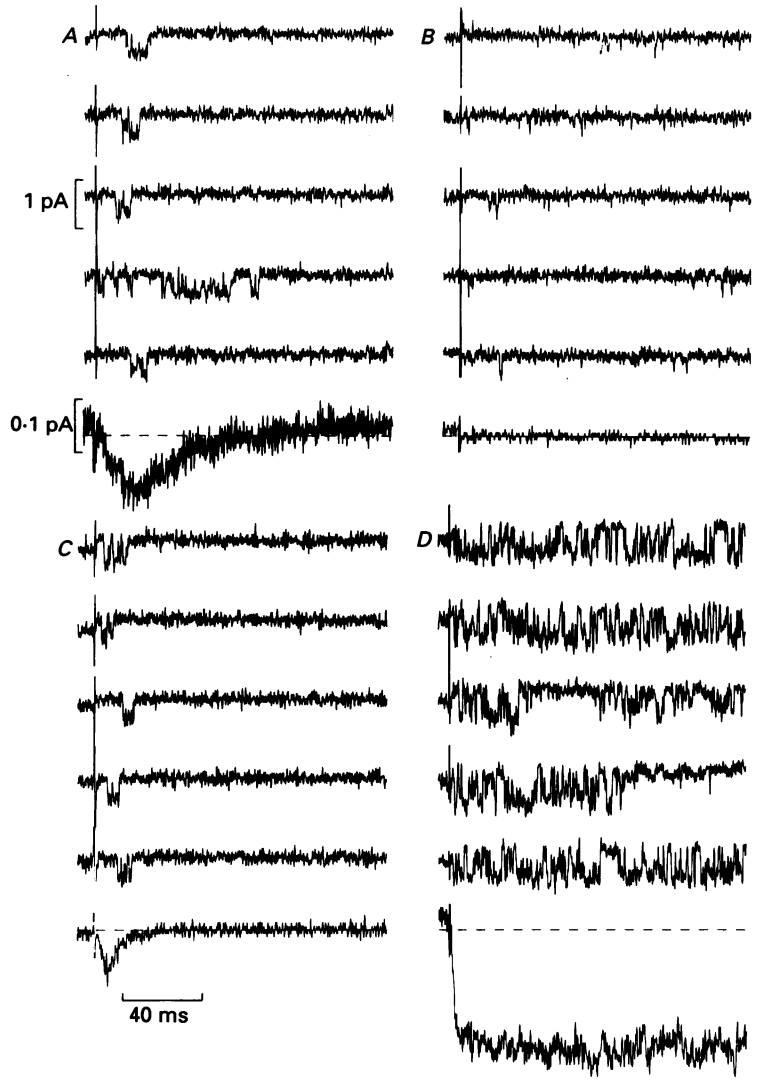

Fig. 1. Different types of cardiac Ca^{2+} channels recorded in 110 mM-$CaCl_2$ or 110 mM-$BaCl_2$. T-type Ca^{2+} channels were activated by a depolarizing step from a holding potential of -100 mV to -20 mV. L-type activity was evoked by a depolarizing step from -40 mV to $+20$ mV. T-type Ca^{2+} channel activity in 110 mM-$CaCl_2$ (*A*) is similar to that in 110 mM-$BaCl_2$ (*C*), whereas the pattern of L-type Ca^{2+} channel activity in 110 mM$CaCl_2$ (*B*) and $BaCl_2$ (*D*) is strikingly different. The scale for the ensemble-averaged current in 110 mM-Ba^{2+} is 0·2 pA; for all other averaged currents it is 0·1 pA. Data filtered at 2 kHz, and sampled at 150 μs intervals.

under the same conditions, i.e. with 110 mM-$CaCl_2$ in the pipette, are characterized by single and very short openings which are dispersed throughout the sweep (panel *B*; see also Fig. 3 in Nilius *et al.* 1985). The mean open time is much less than 1 ms, and the averaged current trace is almost flat. The pattern of T-type channel activity is not strikingly affected when 110 mM-Ba^{2+} is used as the charge carrier (panel *C*).

However, L-type channels evoked from a holding potential of −40 mV under these conditions are bursting throughout the whole sweep. The amplitude of the single-channel current at +20 mV is about 1·5 pA, and the ensemble-averaged current inactivates very slowly (panel *D*). The most straightforward discrimination between T- and L-channel activity can therefore be obtained with 110 mM-$CaCl_2$ in the pipette solution.

We have investigated in total 139 patches, from which twenty-nine showed single-channel activity with no overlapping events. In ten patches simultaneous openings of two channels were observed, and five patches contained at least three channels. The number of channels in each patch was identified with the maximal number of overlapping current events observed in about 2000 sweeps.

This assumption can be justified by the high probability of observing double openings in the beginning of the clamp step if the patch contains more than one channel. At a test potential of −20 mV (see below) Np has a value of 0·08 at the peak of the ensemble-averaged current (N is the number of channels in the patch, and p is the peak open probability of the channel). Assuming $N = 2$ and $p = 0{\cdot}04$, the probability of observing simultaneous openings of both channels in 2000 records is given by $1-(1-p^2)^{2000} \approx 0{\cdot}96$.

A mean value of 0·86 channels per patch was derived from the exponential fit of the distribution of the number of channels per patch. Taking into account the diameter of the pipette and assuming that the membrane area in the pipette equals the tip area, the density of the T-channels in ventricular cells was estimated at 0·1–0·3 μm^{-2}.

The T-type Ca^{2+} channel activity measured at a test potential of −20 mV is characterized by the following parameters (mean values obtained from seven patches). The amplitude of the single-channel current amounts to 0·48 ± 0·02 pA. The peak open probability of the channel, calculated from the peak amplitude of the averaged current and the single-channel current, is 0·08 ± 0·03. The macroscopic time constant of activation (6·0 ± 0·7 ms) is much shorter than the macroscopic time constant of inactivation (28·4 ± 3·3 ms). The mean open time of the channel is 1·7 ± 0·2 ms, compared to a mean closed time of 7·5 ± 2·0 ms. The mean first latency amounts to 20·1 ± 2·1 ms, and the mean burst duration to 11·1 ± 0·5 ms. On average the channel opens 4·8 ± 0·8 times per sweep.

The amplitude of the single-channel currents were obtained by fitting the amplitude histograms to sums of Gaussian distributions (Fig. 2*A*). The current–voltage relationship is linear for test potentials ranging from −50 to +10 mV, as shown in Fig. 2*B*. A slope conductance of 6·8 pS was calculated from the linear regression over all data points.

Openings to a subconductance level were observed in almost every path with T-channel activity (Fig. 3*A*). All possible combinations of transitions could be recorded: separate openings to each level, as well as transitions from the main to the intermediate level, and vice versa. The occurrence of all possible transitions suggests that the T-type Ca^{2+} channel has a substate. Because of these transitions to the sublevel, the open peak in the amplitude histograms is usually better fitted with a sum of two Gaussians than with a single Gaussian, as shown in Fig. 3*B*. This subconductance level has not been further analysed, because of its small amplitude

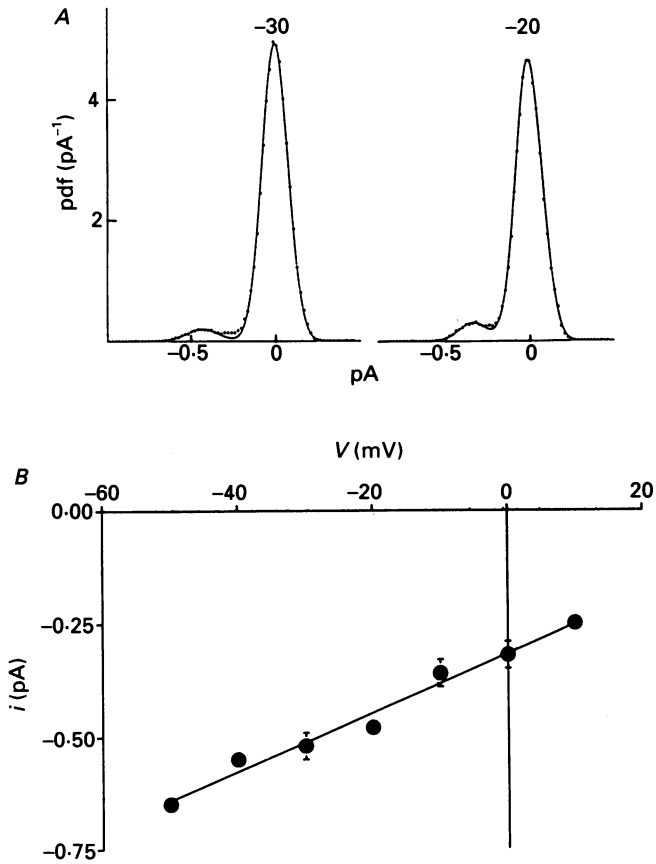

Fig. 2. *A*, amplitude histograms, constructed from non-empty sweeps, at two test potentials. The amplitude histograms were fitted with a sum of Gaussian distributions. Note that the open peak cannot be adequately described by a single Gaussian, suggesting that there might exist a second current level, as seen in Fig. 3. Mean and standard deviation (peak width) of the open peaks are $-0{\cdot}44 \pm 0{\cdot}10$ pA at -30 mV and $-0{\cdot}33 \pm 0{\cdot}09$ pA at -20 mV. The respective probabilities were 0·05 and 0·07. *B*, synopsis of the voltage dependence of the single-channel currents as obtained from amplitude histograms. The data points were obtained from seven patches (one to seven measurements at each test potential). The slope conductance calculated from the linear regression through the data points is 6·8 pS ($r = 0{\cdot}99$).

(about 50% of the main level, range 0·2–0·3 pA) and because of the low frequency of openings.

Activation and inactivation properties of the T-type Ca^{2+} channel

Figure 4 shows a family of single-channel current records and the corresponding ensemble-averaged currents at five different test potentials evoked from the same holding potential of -100 mV. The typical bursting pattern at the beginning of the voltage step, as described in Fig. 1, can be observed. At the more negative test

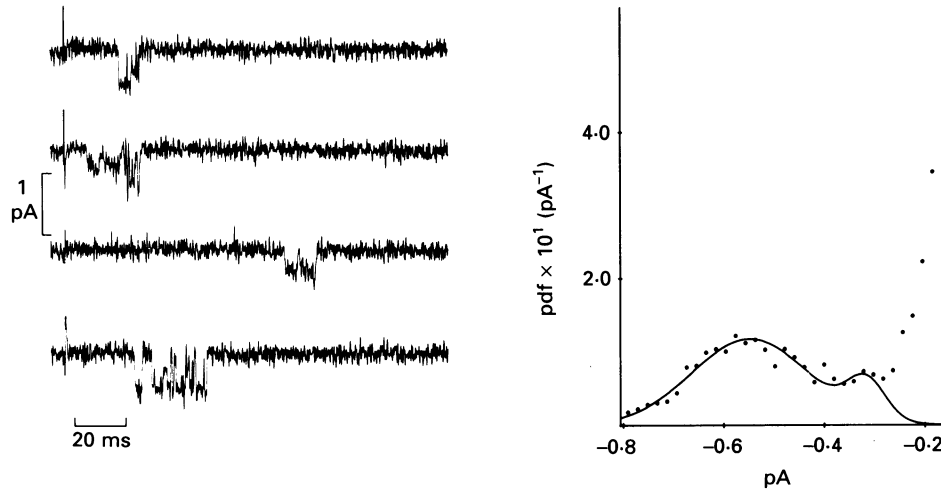

Fig. 3. Openings of the T-type Ca^{2+} channel to subconductance levels. *A*, single-channel currents from one patch showing transitions between two open levels (upper two traces) and separate openings to each level (bottom two traces). *B*, open peak of the amplitude histogram from the same patch as in *A* fitted with two Gaussian distributions (subconductance level: $-0{\cdot}33 \pm 0{\cdot}08$ pA, probability 0·02; main conductance level: $-0{\cdot}54 \pm 0{\cdot}11$ pA, probability 0·06). The closed peak has an amplitude of $0 \pm 0{\cdot}1$ pA, and a probability of 0·92. Holding potential of −100 mV and test potential of −20 mV.

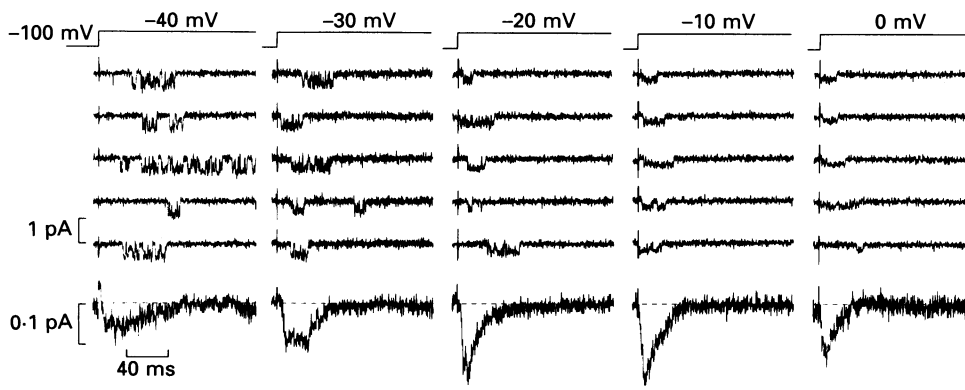

Fig. 4. T-type Ca^{2+} channel currents through single channels and the corresponding ensemble-averaged currents (bottom) obtained at five different test potentials from the same holding potential of −100 mV. Data were filtered at 2 kHz and sampled at 150 μs intervals. Averaged currents were obtained from 194 sweeps.

potentials, the ensemble-averaged current is characterized by a slow activation and inactivation. Both activation and inactivation are clearly voltage dependent, as they become much faster at more positive potentials. The maximal probability P of the channel being open has been estimated from the peaks of the averaged current and from the single-channel current. In spite of the large scatter on the values of the peak current (e.g. at −10 mV the values for P range from 0·08 to 0·21), the voltage

dependence of P could be adequately described by a Boltzmann function (Fig. 5*B*). Half-maximal activation occurs at −14 mV, and the slope parameter s is 10·3 mV. The fitted maximal probability of the channel being open is 0·15.

At less negative holding potentials the peak values of the ensemble-averaged

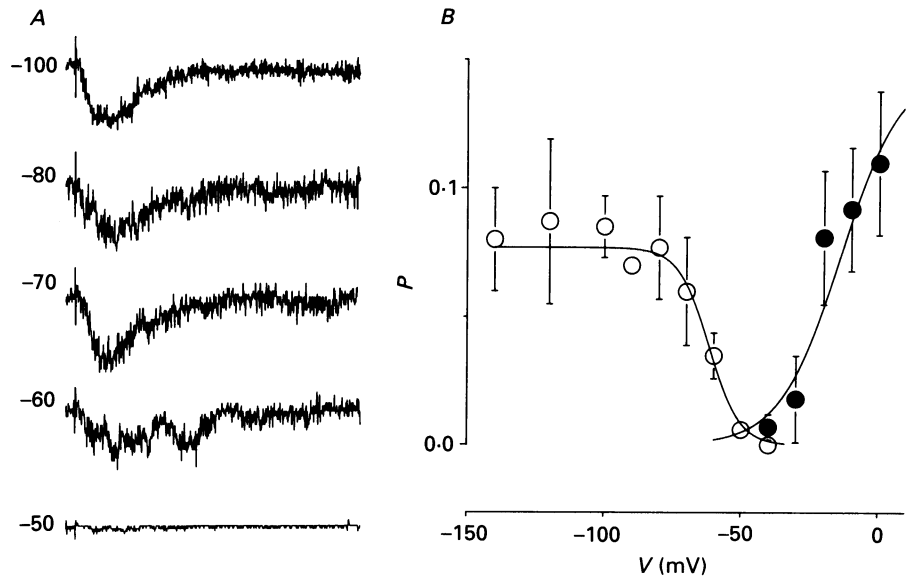

Fig. 5. Steady-state activation and inactivation measured from the ensemble-averaged currents in cell-attached patches. *A*, averaged currents from 194 sweeps for different holding potentials (shown at the left of each trace) at a test potential of −20 mV. Note that inactivation is complete within a voltage range of 20 mV. *B*, pooled data from four cells (twenty-nine data points) for inactivation (○) and five cells (thirty-two data points) for activation (●). The continuous curves represent Boltzmann functions fitted to the data points. Parameters of inactivation: $P_{max} = 0{\cdot}08$, $V_{\frac{1}{2}} = -60{\cdot}7$ mV, $s = 5{\cdot}6$ mV (test potential = −20 mV). Parameters of activation: $P_{max} = 0{\cdot}15$, $V_{\frac{1}{2}} = -14$ mV, $s = 10{\cdot}8$ mV (holding potential = −100 mV).

currents measured at the same test potential are reduced (steady-state inactivation, Fig. 5*A*). This steady-state inactivation could also described by a Boltzmann function with a half-maximal inactivation at −60·7 mV. The slope of the inactivation curve is much steeper than that of activation ($s = 5{\cdot}6$ mV). The maximal P value of 0·08 is consistent with the corresponding value on the activation curve, although a completely different set of experiments was analysed for inactivation.

The rate of decline of the averaged currents also appeared to be very sensitive to the test potential (Figs 4 and 6*A*). The decay of the ensemble-averaged current could be approximated by a single exponential. The time constant of inactivation τ_h decreases monotonically with voltage, as shown in Fig. 6*B*. The time constant of activation τ_a has been determined from the time to peak of the averaged current (t_p) and the time constant of inactivation τ_h (if an m^2h model is assumed, τ_a is the solution of the equation $t_p - \tau_a \ln(2\tau_h/\tau_a + 1) = 0$). The values of τ_a thus calculated range from 9·6 ms at −40 mV, to 8·0 ± 1·9 ms at −30 mV and to 3·7 ± 0·7 ms at 0 mV.

Kinetic analysis of single-channel data

Figure 7 shows a typical example of the kinetic analysis of single-channel data. Panel *A* depicts the typical pattern of T-channel activity consisting of burst-like openings and long waiting times to the first opening. The distribution of the open

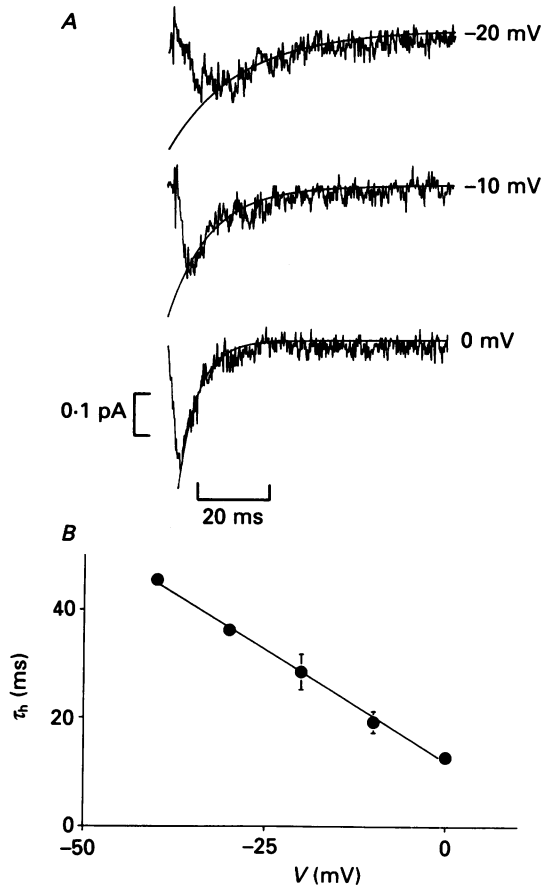

Fig. 6. Voltage dependence of the decay of cardiac T-channel currents. *A*, averaged currents from a holding potential of −100 mV to test potentials of −20, −10 and 0 mV. The decay of the current was fitted with a single exponential (continuous lines) with time constants of respectively 37, 22 and 10 ms. *B*, pooled data from four cells and twenty-three data points showing the voltage dependence of the time constant τ_h of inactivation.

times has been fitted with a single exponential with a time constant $\tau_0 = 1{\cdot}5$ ms (Fig. 7*B*). At least two groups of dwell times in the closed state could be distinguished in the current traces. The closed time probability distribution has therefore been fitted with a sum of two exponentials (Fig. 7*C*; time constants $\tau_f = 0{\cdot}4$ and $\tau_s = 5{\cdot}0$ ms, $N_f = 673$ short closings and $N_s = 238$ long closings). The histogram of the burst duration has been calculated by skipping channel closures shorter than three times the fast time constant of the closed time distribution. This histogram, as shown in Fig. 7*D*, could be fitted with a single exponential with a time constant $\tau_b = 7{\cdot}4$ ms. A total of 203 bursts were observed with, on average, 2·8 openings per burst and

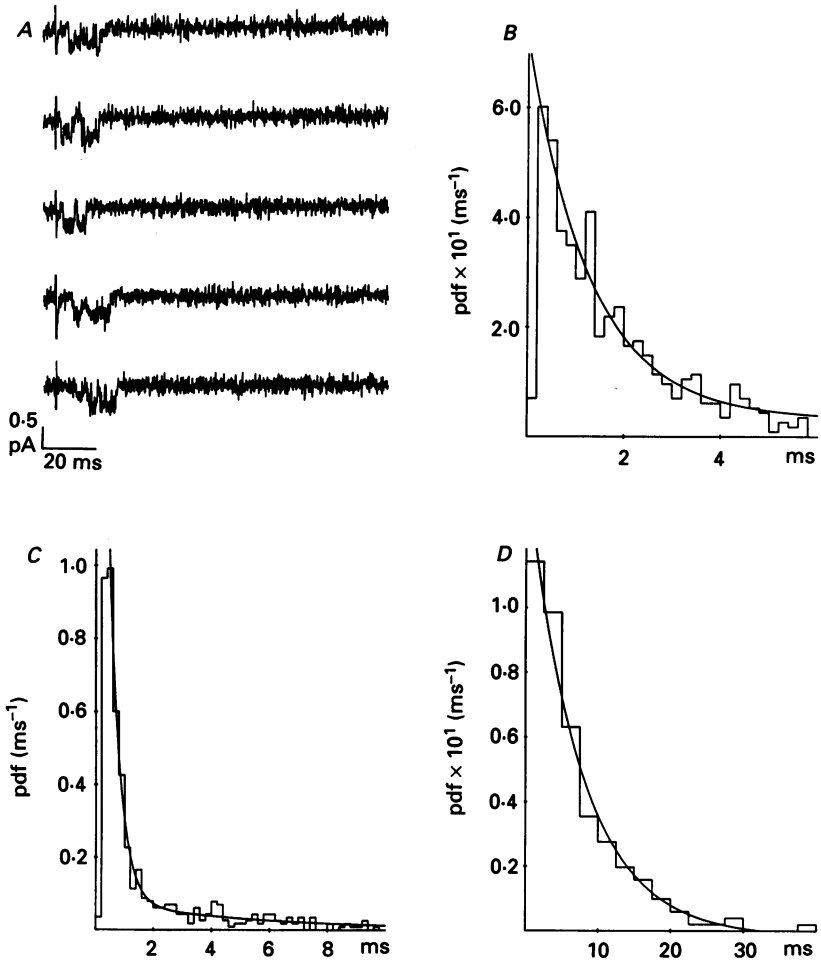

Fig. 7. Kinetic analysis of T-type cardiac Ca^{2+} channel. *A*, single-channel records at a test potential of 0 mV and from a holding potential of −100 mV. *B*, open-time histogram for the data illustrated in *A*. The data were fitted with a single exponential having a mean open time of 1·5 ms (575 events, bin width 0·2 ms). *C*, distribution of the closed times from 575 events and the data illustrated in *A*. The continuous line represents a biexponential fit with time constants of 0·4 and 5·0 ms. The predicted number of fast and long closings amount to 673 and 238 respectively (bin width 0·2 ms). *D*, burst duration distribution measured from 203 events. The time constant of the exponential fit is 7·4 ms (bin width 2·5 ms).

a total mean open time in the burst of 5·6 ms. As a check we have calculated the mean burst duration from the distribution of the observed open time and fast closed-time histograms. The number of observed fast closings (i.e. fast closings longer than $t_D = 0{\cdot}17$ ms) is given by

$$n_f = N_f \exp(-t_D/\tau_f),$$

and the observed number of bursts by,

$$n_b = N - n_f,$$

where N represents the total number of observed closings. The number of openings per burst is

$$n_0 = 1 + n_f/n_b.$$

The mean burst duration μ_b, given by

$$\mu_b = n_0\tau_0 + (n_0 + 1)\tau_f,$$

amounts to 7·8 ms and is in good agreement with the observed value based on our burst definition.

Because the mean open time of the channel is much larger than the dead time of our recording system, it can be assumed that only few openings will be missed, and that the observed mean burst length and the observed number of bursts will be close to their true values. Taking into account all fast openings N_f the true number of openings in a burst is given by

$$N_0 = 1 + N_f/N_b.$$

The value for the mean open time, corrected for missed fast closings, can be obtained by dividing the total open time in the burst by the true number N_0 of openings per burst, and amounts to 1·3 ms, which is about 15% smaller than the value calculated from the open-time histogram.

The voltage dependence of the time constants of the open- and closed-time distributions is shown in Fig. 8. The mean open time does not significantly change with voltage, and a mean open time of $1{\cdot}43 \pm 0{\cdot}14$ ms was calculated from the pooled data. The short mean closed time is also largely voltage independent (mean pooled value of $0{\cdot}48 \pm 0{\cdot}1$ ms), whereas the long closed time increases from 1·9 ms at −50 mV to $8{\cdot}8 \pm 2{\cdot}0$ ms at 0 mV.

The mean burst duration is slightly longer at less negative potentials and ranges from 3·6 ms at −50 mV to 7·0 ms at −40 mV, $6{\cdot}9 \pm 0{\cdot}5$ ms at −30 mV, $8{\cdot}2 \pm 0{\cdot}5$ ms at −20 mV, $10{\cdot}3 \pm 1{\cdot}0$ ms at −10 mV and 7·4 ms at 0 mV.

The distribution of the waiting times to the first opening (first latency) shows a clear-cut peak (Fig. 9*A*), which occurs earlier than the peak of the averaged current. Therefore, channels are opening for the first time when macroscopic inactivation is well underway. The histogram data could be properly described with the function

$$f(t) = c[\exp(-t/\tau_1) - \exp(-t/\tau_2)],$$

which represents the probability density function of waiting times to the first opening for a single-channel patch (Patlak & Horn, 1982). The probability $P(t)$ of finding the channel in the open state t ms after the onset of a voltage step is given by the convolution of the first latency $f(t)$ with the conditional probability of the channel being open at time t given that it first opened at time zero (Aldrich, Corey & Stevens, 1983). We have approximated the latter probability either by the probability of finding an opening with a duration longer than t ms (i.e. $\exp(-t/\tau_0)$), or by the probability of finding a burst duration longer than t ms (i.e. $\exp(-t/\tau_b)$ where τ_b = mean burst duration). These convolutions are shown in Fig. 9*B* together with the open probability as determined from the averaged current. The probabilities calculated from the convolution with the distribution of the open times are too small,

and the peak probability occurs much earlier than the peak-averaged current. This is not unexpected because this approximation does not take into account the reopening of the channel. On the other hand, the convolution of the first latency with the burst duration reasonably fits the averaged current. The small overshoot of the calculated values can be explained by the overestimation of the channel open probability during a burst, which in this approximation is assumed to be 1.

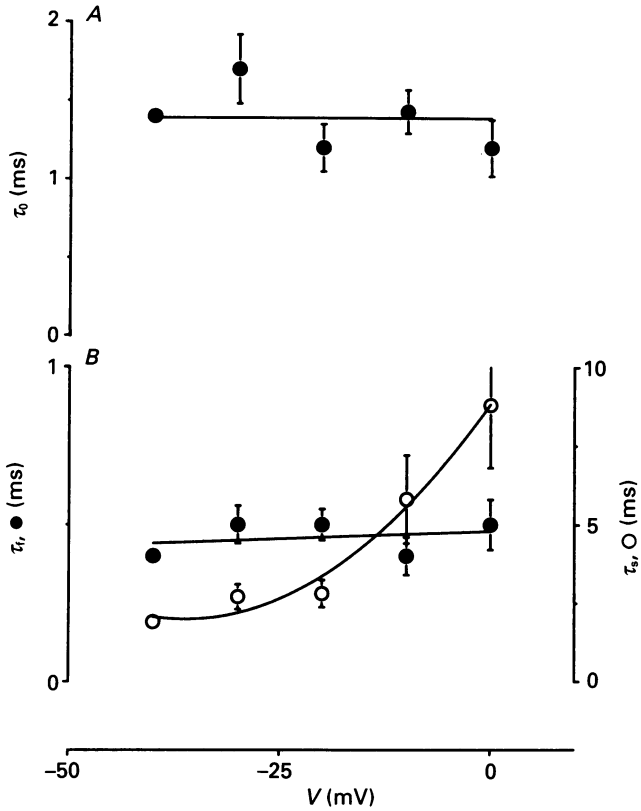

Fig. 8. Voltage dependence of the mean open and mean closed times. *A*, the mean open times as measured from the exponential fits of open time distributions shows no voltage dependence. The mean value over all voltages is 1·43 ± 0·14 ms. *B*, voltage dependence of the mean fast and mean slow closed times. The fast time constant τ_f is voltage independent (0·48 ± 0·1 ms), whereas the slow time constant τ_s increases at more positive voltages.

First-latency histograms were not constructed at all potentials. Instead we have calculated the mean value t_L of the waiting times to the first opening at each potential. These data are represented in Fig. 10*A*, from which it is obvious that t_L is strongly voltage dependent and decreases at more positive potentials. This voltage dependence of t_L is quite similar to that of the macroscopic time constant of inactivation τ_h of the averaged current. The close correlation between both quantities is shown in Fig. 10*B*, where the regression line has a slope of 1·04.

Analysis of the number of openings per sweep

The number of openings per sweep has been analysed in detail for all patches, because the information obtained from this analysis is useful to discriminate between different state models which could possibly describe the kinetics of the channel. The

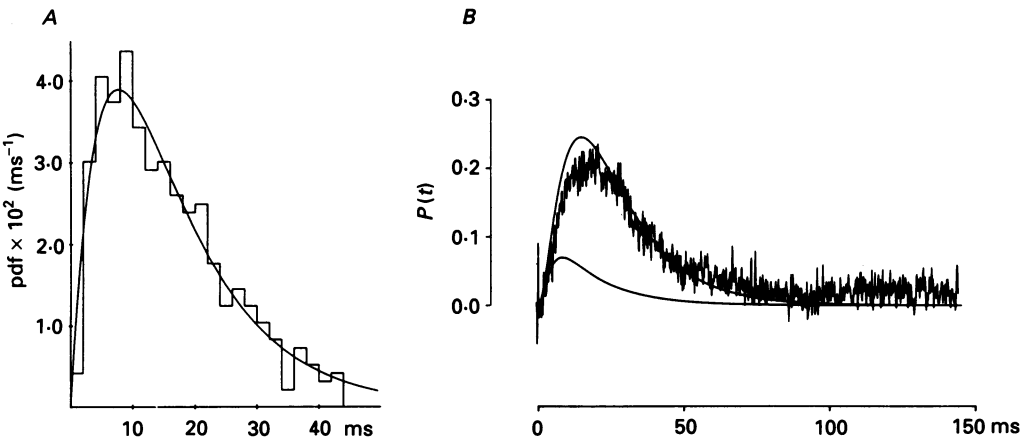

Fig. 9. First-latency distribution and relation between first latency and the probability of the channel being open. *A*. distribution of the first latencies. The histogram has been fitted with the equation $y = c[\exp(-t/\tau_1) - \exp(-t/\tau_2)]$. The time constants of this fit are 5·3 and 11·7 ms. Test potential of −30 mV and holding potential of −100 mV (bin width 2·5 ms). *B*. convolution of the first latency (fitted curve from *A*) with the open time distribution (τ_0 = 1·7 ms, fast decaying continuous line) and with the distribution of the burst duration (τ_b = 7·9 ms). The latter convolution closely fits the probability of the channel being open, as calculated from the averaged current (noisy record). The averaged current was obtained only from the sweeps with openings in order to scale it with the convolutions. The $P(t)$ values are therefore higher than shown in the analysis of steady-state activation and inactivation.

additional information obtained form this analysis includes: (i) the probability p that a channel reopens given that it has opened; (ii) the probability $P(0)$ of observing a record without openings, which will be identified with the probability f that a channel transition bypasses the open state in a given kinetic scheme; (iii) the mean number of openings per sweep $j = (1-f)/(1-p)$.

The kinetics of the T-type Ca^{2+} channel is characterized by a high probability of reopening and a high probability of bypassing the open state. The reopening probability does not depend significantly on the voltage, as can be observed in Fig. 11*A*. A mean value of 0·8±0·01 (n = 26) was calculated from the pooled data. The parameter $P(0)$ or f is more dependent on potential, and shows a minimum value of 0·52±0·03 at −30 mV (Fig. 11*B*). The mean number of openings per non-empty sweep is only slightly voltage dependent (Fig. 11*C*) and increases from 3·9 at −40 mV to 5·8 at 0 mV. The mean value from all data is 4·7±0·3 (n = 26, seven patches).

The probabilities $P(k)$ of finding k openings per sweep, calculated from the above parameters, using the equation

$$P(k) = (1-f)p^{k-1}(1-p),$$

are represented in Fig 11*D*, and closely fit the experimentally observed values.

Modelling of the T-type Ca^{2+} channel kinetics

We have tried to describe the kinetic behaviour of the T-type Ca^{2+} channel by state models, similar to the approach used by Kunze *et al.* (1985) and by Carbone & Lux (1987*a*). The models that have been tested are listed in Table 1. It was assumed in

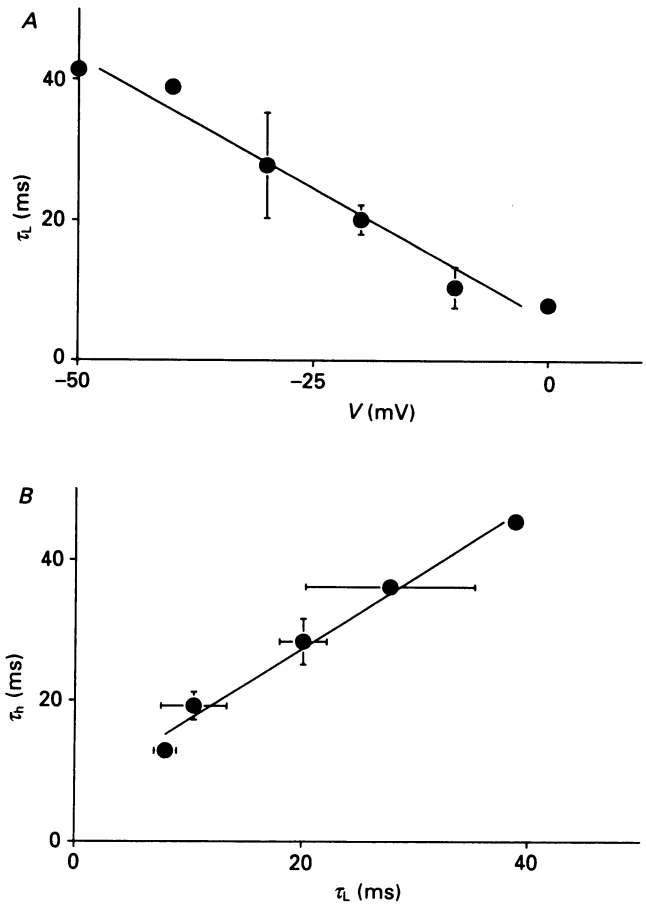

Fig. 10. Correlation between the mean first latencies and the macroscopic time constants of inactivation. *A*, voltage dependence of the mean first latency t_L. The continuous line shows a linear regression. Data were obtained from four patches and twenty-two data points. *B*, correlation between the mean first latency t_L and the time constant of inactivation of the averaged current τ_h. Mean values ± S.E.M. from four patches and twenty-two data points. The slope of the regression line is 1·04 (r = 0·98).

these models that the inactivated state is absorbing. This hypothesis is supported by the observation that the ensemble-averaged current declines to zero at sufficiently long times, suggesting that inactivated channels do not reopen. The considerable fraction of records without openings suggests that closed channels can inactivate, and such an inactivation pathway has therefore been included in all models.

Model M_1, which is the model proposed by Aldrich *et al.* (1983) for the Na^+ channel, is the simplest model that takes into account all these constraints. In this model the absorbing inactivated state can be reached from a single open and from a single

closed state. However, in all patches and at all potentials we have found a value for f greater than 0·5. According to the equations for p and f of this model (see Table 1), p should then have a value less than 0·5, which is in contradiction with our measurements. It is not surprising that this simple model is inconsistent with our

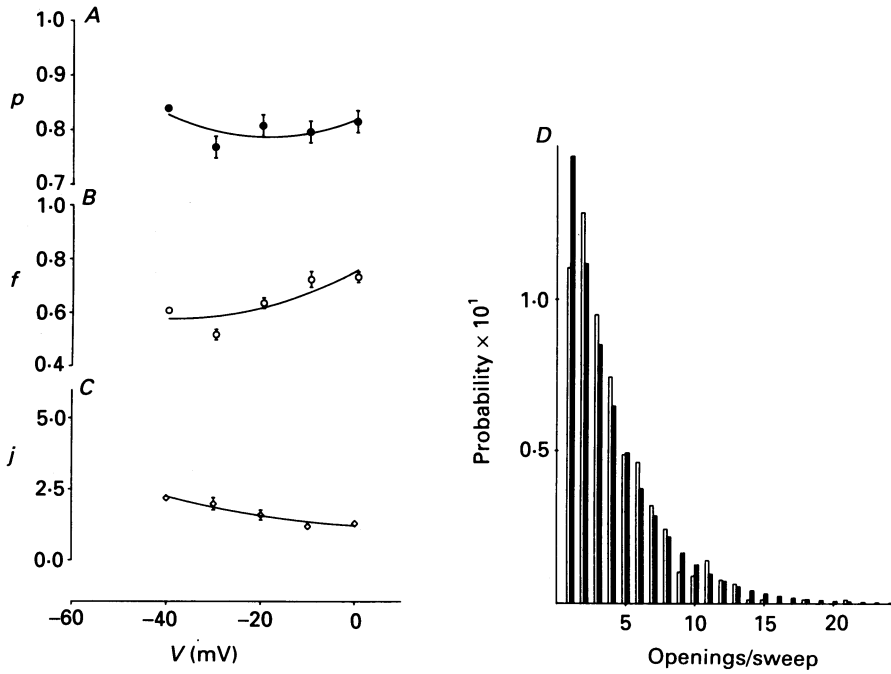

Fig. 11. Voltage dependence of the probability p that the channel can reopen given that it has opened (A), of the probability f of observing a blank record (B) and of the mean number of openings per record j (C). The data were calculated from five patches (twenty-six data points) and corrected for missed fast openings, as described in the Methods. D, distribution of the number of openings per record. The data derived from the experimental records (open histograms) are compared to the theoretical values $P(k)$ of observing k openings (filled histograms), calculated from the probability f of observing a blank record and from the probability P of reopening.

experimental data. The observations that the closed-time histograms could not be fitted with single exponentials and that the first-latency histograms showed a peak indicate that more than one closed state preceeds the open state. However, the more extended model with an additional closed state (model M_2, which is similar to the model used by Vandenberg & Horn, 1984) is also incompatible with our data. The probability B of reaching the absorbing state from the open state in this model can be derived from the expressions for p and f in Table 1, and is given by the equation $B = 1-p/(1-f)$. The values of B, calculated from the experimentally observed values of p and f, were negative in twenty-five out of twenty-six samples from six tested cells, and this model can therefore be rejected. It has to be pointed out that these rejection criteria are even stronger when a large number of short closings are missed: the real values of p would even be higher resulting in more negative values of B.

From the equations for p and f in Table 1 it can be deduced that $p = 1-f$ for

TABLE 1. Markov chain diagrams of the different kinetic models used in this study

Model	Markov chain diagram	Equations
M_1	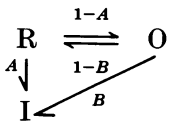	$p = (1-A)(1-B)$ $f = A$
M_2	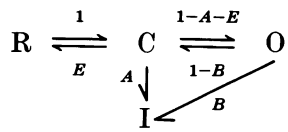	$p = \frac{(1-E-A)(1-B)}{1-E}$ $f = \frac{A}{1-E}$
M_3	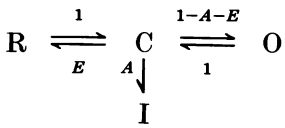	$p = \frac{1-E-A}{1-E}$ $f = \frac{A}{1-E}$
M_4	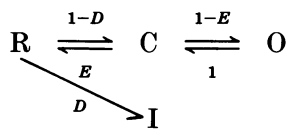	$p = \frac{1-E}{1-E(1-D)}$ $f = \frac{D}{1-E(1-D)}$
M_5	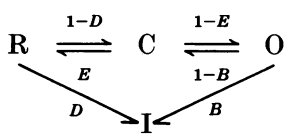	$p = \frac{(1-E)(1-B)}{1-E(1-D)}$ $f = \frac{D}{1-E(1-D)}$
M_6	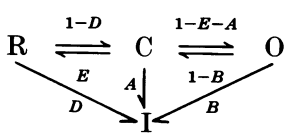	$p = \frac{(1-E-A)(1-B)}{1-E(1-D)}$ $f = \frac{D+A(1-D)}{1-E(1-D)}$

R, C, O and I represent respectively the resting, closed, open and absorbing inactivated states. A, B, D and E represent transition probabilities. These probabilities can be easily calculated from the rate constants of each kinetic scheme by dividing the rate constant of this transition by the sum of the rate constants of all the transitions from the initial state. The equations at the right give the probability of reopening (p) and bypassing the open state (f) for each diagram (Kunze *et al.* 1985), and are used to calculate these parameters from the fitted rate constants in Table 2.

model M_3. This model is therefore incompatible with values of p and f which are both larger than 0·5, and can therefore be rejected. This is not unexpected, because this model does not allow inactivation to occur from the open state. However, the observed close correlation between the time constant of macroscopic inactivation and the first latency provides evidence for such an inactivation pathway proceeding form the open state. For the same reason model M_4 is not very realistic. However, this model has been included because it is easy to get estimates of the rate constants of this model from the experimental data. The transition probabilities D and E can be easily calculated from the equations for p and f in Table 1, and from the number of openings per burst (n_b). It can be easily shown that $E = 1/n_b$, and from the equations of p and f it follows that $D = (1-E)f/p$. The rate constant for each transition can be calculated as the ratio of the corresponding transition probability and the dwell time in the state from which the transition starts, i.e. τ_0, τ_f or τ_s. These estimated values were used as initial values to fit the time course of the open probability $P(t)$ calculated from the ensemble-averaged current for each of the models M_4–M_6, using the fit procedure as described in the Methods. Only records with a sufficiently negative holding potential to reduce steady-state inactivation were used, so that it can be assumed that the channel is in the long-lived closed state at rest. In model M_6 it was assumed that inactivation is independent of activation, and hence that the rate constant for inactivation is the same from each state in the activation pathway. Figure 12*A–C* shows the measured and fitted open probabilities for each of the kinetic schemes M_4–M_6. Each model describes the time course of the open probability $P(t)$, but the predicted time courses for each model are hardly different in spite of the large differences between the corresponding rate constants of each model, as shown in Table 2. From these rate constants we have calculated a number of parameters, which can be easily verified with experimentally observed quantities. These are also summarized in Tables 2 and 3 and are in reasonable agreement with the experimentally observed values. The analysis based on model fitting of ensemble-averaged currents does not therefore allow discrimination between these different models. A possible reason for this failure might be that the predicted time course of $P(t)$ is not very sensitive to changes of the rate constants of the model. This might explain why the predicted time courses for each model are similar in spite of the large differences between the corresponding rate constants. This assumption is supported by the findings that simulated time courses of $P(t)$ for models M_4–M_6 could usually be fitted equally well with each model, and that the final values of the rate constants strongly depend on their initial guessed values.

The fitted rate constants of models M_5 and M_6 have therefore only been used to estimate the effect of limited time resolution on the kinetic parameters derived from our experimental data. Based on these rate constants we have simulated single-channel dwell times, and incorporated the effect of missed short events by adding all events which are shorter than some critical duration (0·17 ms in our experiments) to the preceding dwell time. These simulated data were analysed in a similar way to the experimental data, and the derived kinetic parameters were compared to those obtained with simulated data without missed events. Missing short events results in overestimates of the mean open time by 35%, and underestimates of the mean number of openings per record and per burst by 25–30%. All other parameters were

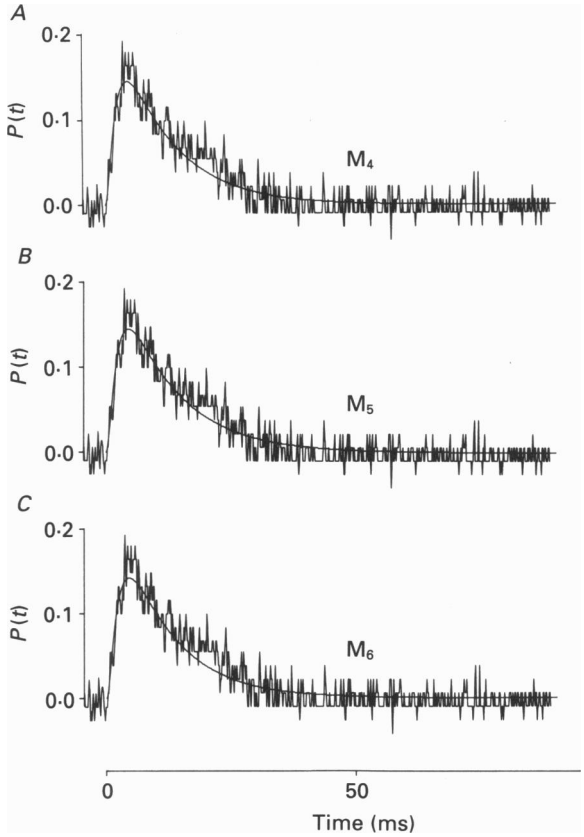

Fig. 12. Probability of the channel being open, calculated from the ensemble-averaged current and the single-channel current, compared to the fitted probability from the kinetic schemes M_4–M_6. Averaged current calculated from 194 records of single-channel currents at 0 mV from a holding of −100 mV.

TABLE 2. Rate constants, expressed in s^{-1}, obtained by fitting the time course of the open probability of the kinetic schemes M_4–M_6

	M_4	M_5	M_6
k_{RI}	87	93	73
k_{RC}	35	27	25
k_{CR}	571	186	200
k_{CO}	1561	2437	3202
k_{OC}	477	531	564
k_{OI}	—	65	73
k_{CI}	—	—	73

k_{ij} with i, j = R, C, O or I represents the rate constant from state i to state j.

TABLE 3. Comparison of the experimental values for the reopening probability (p), the probability (f) of observing a blank record, the mean number of openings per record (j), and the mean dwell times in the open (τ_0), short-lived (τ_f) and long-lived (τ_s) closed states with the values predicted from the fitted rate constants of models M_4–M_6; p and f are calculated by the equations given in Table 1, j is given by the ratio $(1-f)/(1-p)$, and the dwell times are given by the inverse sum of the rate constants leaving these states

	Experiment	M_4	M_5	M_6
p	0·82	0·79	0·84	0·83
f	0·74	0·77	0·79	0·76
j	1·44	1·10	1·34	1·39
τ_0	1·41	2·1	1·68	1·57
τ_f	0·40	0·47	0·38	0·29
τ_s	6·1	8·2	8·3	10·2

only marginally affected. The arguments which we have used to eliminate models M_1–M_4 are therefore not invalidated by the limited time resolution of our experimental data.

DISCUSSION

In the present paper we have analysed the kinetic properties of the gating of the cardiac T-type Ca^{2+} channel. Until now such an analysis was not available for cardiac muscle, and it is worthwhile to compare the single-channel kinetics presented in this paper with the T-type Ca^{2+} channel activity in other tissues (Carbone & Lux, 1987*a*).

Macroscopic and single-channel data

In our study single-channel currents were recorded in the voltage range between −50 and +10 mV. However the analysis was mainly limited to data obtained in the range from −40 to 0 mV because of the large number of empty records at −50 mV and the small amplitude of the single-channel current at +10 mV.

The slope conductance of 6·8 pS in 110 mM-$CaCl_2$ found in this study is consistent with the previously reported values for the T-type Ca^{2+} channel (heart muscle: Nilius *et al.* 1985; Hagiwara *et al.* 1988; DRG neurones: Nowycky, Fox & Tsien, 1985; Carbone & Lux, 1987*a*; Fox *et al.* 1987*b*; smooth muscle: Benham, Hess & Tsien, 1987).

In most patches two levels of unitary currents with a different probability of occurrence could be detected. The subconductance level is about 50% of the main level, but because of the low frequency of transitions to the sublevel it can be excluded that the openings to the main level represent simultaneous openings of two channels to the sublevel. On the other hand all possible transitions between the two open levels and the closed level were observed. The existence of two open states of the same channel is therefore more likely than the presence of two types of channels in the patch. A substate for the T-channel has also been described in DRG cells (Carbone & Lux, 1987*b*): the main level is about 1·5 times the sublevel, and the frequency of transitions to the sublevel is higher than in our experiments. The existence of substates seems therefore to be the rule rather than the exception, and

has already been described for the L-type Ca^{2+} channel (Prod'hom, Pietrobon & Hess, 1987; Pietrobon, Prod'hom & Hess, 1988) and for the voltage-gated Na^+ channel in heart muscle (Kohlhardt, Frobe & Herzig, 1987; Scanley & Fozzard, 1987; Nilius, Vereecke & Carmeliet, 1989).

The ensemble-averaged current is characterized by a strongly voltage-dependent steady-state activation and inactivation. The absolute value for the peak open probability of 0·15 is considerably smaller than that for the L-type Ca^{2+} channel in the same tissue (0·47–0·84: Cavalié, Pelzer & Trautwein, 1986). The voltage dependence of inactivation is steeper than that for activation, similar to the findings in DRG cells (Fox *et al.* 1987*b*). The slope parameter of the activation curve in our experiments is larger than the value obtained from whole-cell currents in other cells (6·5 mV: Fox *et al.* 1987*a*; 7 mV: Fox *et al.* 1987*b*; 6·1 mV: Hagiwara *et al.* 1988; but 15 mV: Cota, 1986), whereas the slope of the activation curve is rather similar (5 mV: Benham *et al.* 1987; 6·6 mV: Hagiwara *et al.* 1988). The time course of activation and inactivation of T-type Ca^+ channels in ventricular cells (this study) is slower than in atrial cells (Hagiwara *et al.* 1988), but faster than in DRG cells (Fox *et al.* 1987*a*).

The macroscopic time constant of inactivation shows a close correlation with the mean first latency, but such a correlation with, for example, the mean open time or the mean burst duration is completely absent. This observation therefore suggests that macroscopic inactivation is at least partially controlled by the microscopic activation.

The values of mean open and closed times reported in this paper are in the same range of those obtained in DRG cells (Carbone & Lux, 1987*b*), but the mean burst duration is markedly shorter than in DRG cells (59 ms at −40 mV).

Microscopic kinetic behaviour of the cardiac T-type Ca^{2+} channel

The typical kinetic properties of the T-type Ca^{2+} channel are: (i) clusterings of openings at the beginning of a depolarizing pulse, which results in a fast activation and inactivation; (ii) openings occurring in bursts, i.e. channel activation with a high probability of reopening, but a low probability of a second burst per sweep (the probability of the occurrence of a second burst if one burst has already been observed is less than 8%); (iii) a high probability of observing blanks; and (iv) a long-lasting and strongly voltage-dependent first latency.

The first-latency distribution shows a maximum that appears earlier than the peak of the averaged current. If macroscopic inactivation is exclusively due to late single openings, one would expect a close correlation between the normalized averaged current and the convolution of the first latency with the open time distribution (Aldrich *et al.* 1983). This is certainly not the case for the cardiac T-type Ca^{2+} channel (see Fig. 9). However, a much better correlation exists if the convolution of the first latency with the distribution of the burst duration is taken. This finding suggests that activation and inactivation are not strongly coupled: the voltage dependence of activation is controlled by the voltage dependence of the first latency, and macroscopic inactivation is due to the late appearance of a burst of openings.

Inactivation at the single-channel level

The kinetic schemes of the T-type Ca^{2+} channels, in which the absorbing inactivated state can be reached from the open state only, could be excluded. These models are not consistent with the measured high probability p of reopening and the high probability f of bypassing the open state. Also the models in which transitions between open and absorbing state do not occur, are very unlikely because they cannot explain the close correlation between first latency and time constant of macroscopic inactivation. Model M_5 and M_6 describe the kinetic data equally well, but our analysis does not allow us to discriminate between both models. The strong voltage dependence of the first latency and the voltage independence of the mean open and short-closed dwell times suggest that the voltage dependence of the T-type Ca^{2+} channel kinetics mainly resides in the transitions between resting and short-lived closed states.

The microscopic behaviour of the T-type Ca^{2+} channel is therefore different from the gating behaviour of the fast inactivating Na^+ channels (Aldrich *et al.* 1983; Horn, Vandenberg & Lange, 1984; Horn & Vandenberg, 1984; Vandenberg & Horn, 1984; Kunze *et al.* 1985) and the L-type Ca^{2+} channel (Brum, Osterrieder & Trautwein, 1984; Cavalié *et al.* 1986; Reuter, Kokubun & Prod'hom, 1986). An intriguing question is whether the obvious differences in the kinetic schemes of different ionic channels from the same superfamily of voltage-operated channels are reflected in their molecular topology.

We thank Professor E. Carmeliet for his generous support of this work and valuable discussions. We are also grateful to Mr J. Prenen for his help during the experiments.

REFERENCES

ALDRICH, R. W., COREY, D. P. & STEVENS, C. F. (1983). A reinterpretation of mammalian sodium channel gating based on single channel recording. *Nature* **306**, 436–441.

BEAN, B. P. (1985). Two kinds of calcium channels in canine atrial cells. *Journal of General Physiology* **86**, 1–30.

BENHAM, CH. D., HESS, P. & TSIEN, R. W. (1987). Two types of calcium channels in single smooth muscle cells from rabbit ear artery studied with whole-cell and single channel recordings. *Circulation Research* **61**, suppl. I, I10–16.

BONVALLET, R. (1987). A low threshold calcium current recorded at physiological Ca concentrations in single frog atrial cells. *Pflügers Archiv* **408**, 540–542.

BRUM, G., OSTERRIEDER, W. & TRAUTWEIN, W. (1984). β-Adrenergic increase in the calcium conductance of cardiac myocytes studied with the patch clamp. *Pflügers Archiv* **401**, 111–118

CARBONE, E. & LUX, H. D. (1984). A low voltage-activated, fully inactivated Ca channel in vertebrate sensory neurones. *Nature* **310**, 501–502.

CARBONE, E & LUX, H. D. (1987*a*). Single low-voltage-activated calcium channels in chick and rat sensory neurones. *Journal of Physiology* **386**, 571–601.

CARBONE, E. & LUX, H. D. (1987*b*). Kinetics and selectivity of a low-voltage-activated calcium current in chick and rat sensory neurones. *Journal of Physiology* **386**, 547–570.

CAVALIÉ, A., PELZER, D. & TRAUTWEIN, W. (1986). Fast and slow gating behaviour of single calcium channels in cardiac cells. Relation to activation and inactivation of calcium-channel current. *Pflügers Archiv* **406**, 241–258.

COTA, G. (1986). Calcium channel currents in pars intermedia cells of the rat pituitary gland. *Journal of General Physiology* **88**, 83–105.

DEITMER, J. W. (1984). Evidence for two voltage-dependent calcium currents in the membrane of the ciliate *Stylonychia*. *Journal of Physiology* **355**, 137–159.

DE RIEMER, S. A. & SAKMANN, B. (1986). Two calcium currents in normal rat anterior pituitary cells identified by a plaque assay. *Experimental Brain Research* **14**, 139–154.

FOX, A. P., NOWYCKY M. C. & TSIEN, R. W. (1987*a*). Kinetic and pharmacological properties distinguishing three types of calcium currents in chick sensory neurones. *Journal of Physiology* **394**, 149–172.

FOX, A. P., NOWYCKY M. C. & TSIEN, R. W. (1987*b*). Single-channel recordings of three types of calcium channels in chick sensory neurones. *Journal of Physiology* **394**, 173–200.

HAGIWARA, N., IRISAWA, H. & KAMEYAMA, M. (1988). Contribution of two types of calcium currents to the pacemaker potentials of rabbit sino-atrial node cells. *Journal of Physiology* **395**, 233–253.

HAMILL, O. P., MARTY, A., NEHER, E., SAKMANN, B. & SIGWORTH, F. J. (1981). Improved patch-clamp techniques for high-resolution current recording from cells and cell-free membrane patches. *Pflügers Archiv* **391**, 85–100.

HIRIART, M. & MATTESON, D. R. (1988). Na channels and two types of Ca channels in rat pancreatic B cells identified with the reverse hemolytic plaque assay. *Journal of General Physiology* **91**, 617–639.

HORN, R. & VANDENBERG, C. A. (1984). Statistical properties of single sodium channels. *Journal of General Physiology* **84**, 505–534.

HORN, R. VANDENBERG, C. A. & LANGE, K. (1984). Statistical analysis of single sodium channels. Effects of *N*-bromoacetamide. *Biophysical Journal* **45**, 323–335.

KOHLHARDT, M., FROBE, U. & HERZIG, J. W. (1987). Properties of normal and non-inactivating single cardiac Na^+ channels. *Proceedings of the Royal Society* B **232**, 71–93.

KUNZE, D. L., LACERDA, A. E., WILSON, D. L. & BROWN, A. M. (1985). Cardiac Na currents and inactivating, reopening, and waiting properties of single cardiac Na channels. *Journal of General Physiology* **86**, 671–719.

LLINÁS, R. & YAROM, Y. (1981). Properties and distribution of ionic conductances generating electroresponsiveness of mammalian inferior olivary neurones *in vitro*. *Journal of Physiology* **315**, 569–584.

MCCLESKEY, E. W., FOX, A. P., FELDMAN, D. & TSIEN, R. W. (1986). Different types of calcium channels. *Journal of Experimental Biology* **124**, 177–190.

MACKIE, G. O. & MEECH, R. W. (1985). Separate sodium and calcium spikes in the same axon. *Nature* **313**, 791–793.

MITRA, R. & MORAD, M. (1985). A uniform enzymatic method for dissociation of myocytes from heart and stomachs of vertebrates. *American Journal of Physiology* **249**, H1056–1060.

MITRA, M. & MORAD, M. (1986). Two types of calcium channels in guinea-pig ventricular myocytes. *Proceedings of the National Academy of Sciences of the USA* **83**, 5340–5344.

NILIUS, B. (1986). Possible functional significance of a novel type of cardiac Ca channel. *Biomedica et biochimica acta* **45**, K37–45.

NILIUS, B., HESS, P., LANSMAN, J. B. & TSIEN, R. W. (1985). A novel type of cardiac calcium channel in ventricular cells. *Nature* **316**, 443–446.

NILIUS, B., HESS, P., LANSMAN, J. B. & TSIEN, R. W. (1986). Two types of Ca channels in isolated ventricular cells from guinea pig heart. *Progress in Zoology* **33**, 75–82.

NILIUS, B., VEREECKE, J. & CARMELIET, E. (1989). Different conductance states of the bursting Na channel in guinea-pig ventricular myocytes. *Pflügers Archiv* **413**, 242–248

NOWYCKY, M. C., FOX, A. P. & TSIEN, R. W. (1985). Three types of neuronal calcium channel with different calcium agonist sensitivity, *Nature* **316**, 440–443.

PATLAK, J. B. & HORN, R. (1982). The effect of *N*-bromoacetamide on a single sodium channel currents in excised membrane patches. *Journal of General Physiology* **79**, 333–351.

PIETROBON, D., PROD'HOM, B. & HESS, P. (1988). Conformational changes associated with ion permeation in L-type calcium channels. *Nature* **333**, 373–376.

PROD'HOM B., PIETROBON, D. & HESS, P. (1987). Direct measurement of proton transfer rates to a group controlling the dihydropyridine-sensitive Ca^{2+} channel. *Nature* **329**, 243–246.

REUTER, H., KOKUBUN, S. & PROD'HOM, B. (1986). Properties and modulation of cardiac calcium channels. *Journal of Experimental Biology* **124**, 191–201.

SAKMANN, B. & NEHER, E. (1983). Geometric parameters of pipettes and membrane patches. In *Single Channel Recording*, ed. SAKMANN, B. & NEHER, E., pp. 37–51. New York, Plenum Press.

SATIN, L. S. & COOK, D. L. (1988). Evidence for two calcium currents in insulin-secreting cells. *Pflügers Archiv* **411**, 401–409.

SCANLEY, B. E. & FOZZARD, H. A. (1987). Low conductance sodium channels in canine cardiac Purkinje cells. *Biophysical Journal* **52**, 489–495.

TYTGAT, J., NILIUS, B., VEREECKE, J. & CARMELIET, E. (1988). The T-type Ca channel in guinea-pig ventricular myocytes is insensitive to isoproterenol. *Pflügers Archiv* **411**, 704–706.

VANDENBERG, C. A. & HORN, R. (1984). Inactivation viewed through single sodium channels. *Journal of General Physiology* **84**, 535–564.